Nanoscale

REVIEW

View Article Online
View Journal | View Issue



Cite this: *Nanoscale*, 2015, **7**, 6409

# Color generation *via* subwavelength plasmonic nanostructures

Yinghong Gu,[a] Lei Zhang,[a] Joel K. W. Yang,[b,c] Swee Ping Yeo[a] and Cheng-Wei Qiu*[a]

Received 26th January 2015,
Accepted 13th March 2015

DOI: 10.1039/c5nr00578g

www.rsc.org/nanoscale

Recent developments in color filtering and display technologies have focused predominantly on high resolution, color vibrancy, high efficiency, and slim dimensions. To achieve these goals, metallic nanostructures have attracted extensive research interest due to their abilities to manipulate the properties of light through surface plasmon resonances. In this paper, we review recent representative developments in plasmonic color engineering at the nanoscale using subwavelength nanostructures, demonstrating their great potential in high-resolution and high-fidelity color rendering, spectral filtering applications, holography, three-dimensional stereoscopic imaging, *etc*.

## 1. Introduction

In nature, colors are mainly produced by the light scattering or partial absorption of materials. Color displays such as emissive liquid-crystal displays employ pigment-based color filters to absorb the complementary colors to produce the red, green, and blue channels.[1–3] With the drive towards higher-resolution imaging and displays, new innovations are needed to achieve higher resolution, lower power consumption, higher compactness, and also color tunability in devices. The highest possible resolution in theory for color display and imaging is set by the diffraction limit of the accompanying optics,[4] which is ~250 nm pitch for imaging through high numerical-aperture objectives with visible light. However, the resolution of the existing pigment-based color printing can just reach the level of ten micrometers, still 1 or 2 orders away from this target.

Alternatively, colors can also be generated by structure engineering, such as diffraction optic devices, photonic crystals, and plasmonic structures. Some naturally occurring photonic structures generate the colorful appearance of some types of insects, birds and aquatic animals,[5–12] usually with the combined effects of thin film/multilayer interferences, grating diffraction, photonic crystals and light scattering. An example of natural structural color is butterfly wings, which has been widely investigated and reproduced through nanostructures fabricated in labs.[7–12] It has been demonstrated that this structural color effect based on photonic crystals, nanowire arrays and polycarbonate (PC) or other dielectric multilayered nanostructures can be useful in optical applications,[13–18] such as color generation by the patterned arrays of silicon nanowires[13–15] and nanowire-based wavelength selective photodetectors.[16]

However, the size of unit cells of these non-plasmonic nanostructures is in the order of the wavelength of light, usually in micrometer dimensions. This means that there is still room for further improvements to reach the diffraction limit. To go beyond the natural color generation, surface plasmon resonances (SPRs) open a promising way to control colors with high efficiency and high resolution due to the development of nano-fabrication technologies. The interaction between light and plasmonic nanostructures has been shown to manipulate the intensity, phase, and polarization of scattering light.[19–27] Thus plasmonic nanostructures are promising for use in high-resolution color displays and imaging applications due to their small dimensions and the ability to manipulate light efficiently.[28–30] The sub-wavelength plasmonic elements enable the structure to be ultra-thin, usually 1–2 orders of magnitude thinner than pigment-based filters, making it favourable for integration and miniaturization of display devices. Plasmonic color filters with a periodic subwavelength hole array in a metal film can achieve high transmission efficiencies due to the phenomenon of extraordinary optical transmission (EOT),[19,20,22,31] which is an important consideration in reducing power consumption. Moreover, the energy absorbed by a multi-layered nano-grating filter can be harvested and converted to electrical energy while producing desirable colors in the visible band,[32] making it energy-efficient and suitable for electro-optic applications. Recently, color printing with plasmonic nanostructures has demonstrated the resolution of 100 000 dots per inch (d. p. i.), which is already at the diffraction limit.[33] This high-resolution

[a]*Department of Electrical and Computer Engineering, National University of Singapore, Singapore 117583, Singapore. E-mail: chengwei.qiu@nus.edu.sg*
[b]*Institute of Materials Research and Engineering, Agency for Science, Technology and Research, 3 Research Link, Singapore 117602, Singapore*
[c]*Singapore University of Technology and Design, Engineering Product Development, Singapore 138682, Singapore*

plasmonic color printing technology has significance in optical data storage, digital imaging, and in security applications. In addition, although some plasmonic nanostructures are designed to avoid incident angle dependence,[34] it is also useful for developing active color filters with controllable output based on sensitivities to the incident angle or polarization.[35,36] With these advantages, the plasmonic nanostructures have great potential in color filtering and imaging applications such as digital photography and digital displays.

This paper provides an overview of the most recent development of nanostructural color filtering and imaging nanotechnologies, and several kinds of representative nanostructures that perform well in color filtering and imaging or that have special functionalities are presented. We discuss the advantages and potential for practical applications as well as their limitations.

## 2. Color generation of plasmonic nanostructures

Surface plasmons (SPs) are collective free-electron oscillations at the metal-dielectric interfaces. They exhibit enhanced near-field amplitude of the electric field at the resonance wavelength. This field is highly localized and decays exponentially away from the metal–dielectric interface.[37–41] Unlike the photon absorption in pigments, which is determined by the energy level transitions of the molecules, the scattering and absorption of plasmonic nanostructures are determined by their geometry and dimensions. Leveraging on the development of nanofabrication technologies such as electron-beam lithography (EBL) and focused ion beam (FIB), the shape and size of metallic nanostructures can be well-controlled with sub-10 nm precision.[42,43] With these sub-wavelength elements, the pixels of color imaging can be extremely small and the resolution can be improved up to the diffraction limit, with a thickness of the resonators of only tens of nanometers. In addition to the advantage of high resolution and ultrathin characteristics, plasmonic nanostructures have also the following attributes: (1) as the nanostructures are made of metal, they are chemically stable and can endure long-duration ultraviolet irradiation and high temperatures compared to chemical pigments; (2) the device can realize a broad range of colors using a single element of metals, by just varying the lateral size and geometry of the structures. This avoids the sequential deposition of inks and reduces the process steps and misalignment between the color channels; (3) the SPRs can be tuned by factors such as the environment index, the incident angle and polarization, and it is possible to make the optical element active,[35,36,44–48] which could be useful for a dense optical data archival,[49] and contributes to security applications.

### 2.1 Structural color from the localized surface plasmon resonance (LSPR)

**2.1.1 Polarization-independent nanoantennas.** Well-designed plasmonic nanoparticles can be viewed as optical nanoantennas that receive optical radiation from the far field to the near field at specific frequencies and *vice versa*. Due to the geometry- and dimension-dependence, the localized surface plasmon resonances (LSPR) of these nanoantennas can be manipulated to achieve the desirable reflection and transmission spectra,[35,46,50,51] and further generate the imaging pattern with pre-designed plasmonic structures.[21,52,53] A typical reflection-mode plasmonic color filter based on the silver vertical nanorod array[50] is shown in Fig. 1. To understand the mechanism, each single nanorod can be modeled by a dipole of polarizability $\alpha$, and the LSPR can be estimated by

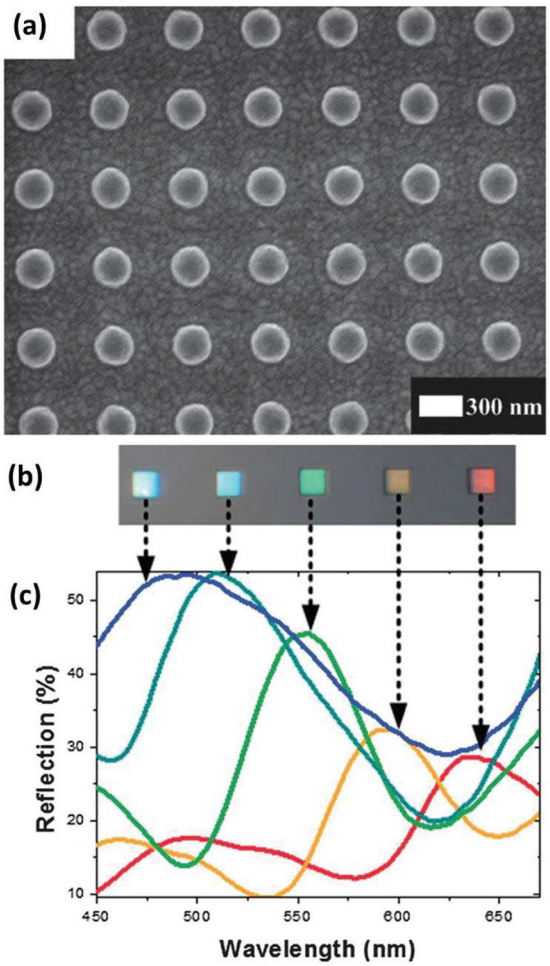


| Presented color | Periodicity (nm) | Rod diameter (nm) | Gap (nm) | $d/p$ |
|---|---|---|---|---|
| Red | 540 | 500 | 40 | 0.926 |
| Yellow | 485 | 450 | 35 | 0.928 |
| Green | 430 | 400 | 30 | 0.930 |
| Cyan | 375 | 350 | 25 | 0.933 |
| Blue | 320 | 300 | 20 | 0.938 |

**Fig. 1** (a) Scanning electron microscope (SEM) image of the top view of Ag vertical nanorod arrays on a quartz substrate with a periodicity $p$ = 550 nm. (b) Optical image of the reflective colors from different Ag nanorod arrays. (c) Measured reflection spectra of the corresponding arrays as a function of wavelengths. The table below (c) shows the size parameters of nanostructures for different colors in (b) and (c). Reproduced with permission.[50] Copyright 2013, RSC.

the coupling dipole theory.[54,55] When the resonator is excited, it radiates a scattering field in proportion to its dipole moment. The static polarizability of each resonator can be written as[56,57]

$$\alpha^{\text{static}} \propto V \frac{\varepsilon_m - \varepsilon_d}{3\varepsilon_m + 3\chi(\varepsilon_m - \varepsilon_d)} \quad (1)$$

where $\varepsilon_m$ and $\varepsilon_d$ are the relative permittivities of the metal and surrounding environment, respectively; $\chi$ is the geometrical factor relating to the physical shape of a nanorod and $V$ is the volume of a resonator. Assuming that the whole array is infinite, the effective polarizability $\alpha^*$ of the LSPR on a single dipole resonator can be generally expressed as[57]

$$\alpha^* = \frac{1}{\frac{1}{\alpha} - S} \quad (2)$$

where the array factor $S$ for the square array with normal incidence can be written as[57]

$$S = \sum_{\text{dipoles}} e^{ikr}\left[\frac{(1-ikr)(3\cos^2\theta - 1)}{r^3} + \frac{k^2\sin^2\theta}{r}\right] \quad (3)$$

where $\theta$ and $r$ denote the position of dipole resonators. When the condition $S = 1/\alpha$ is satisfied, the effective polarizability would be maximized, leading to a resonance of the dipole array with strong scattering. The wave scattering backward at the resonance results in a reflected peak, and a transmitted dip correspondingly. Although the collective plasmonic resonances are also influenced by the Wood's anomaly and Bloch wave surface plasmon polaritons,[58–62] which are mutually coupled and may even lead to the anti-crossing effect.[63,64] These expressions provide a good estimate for the color filtering mechanism of the nanoantenna array.

The dimension of the nanorods in Fig. 1a is optimized to enhance efficiency, and the reflected color is controlled by the diameter and periodicity of the nanorod array. To achieve the full color band, especially the blue color, a small periodicity and high diameter/periodicity ($d/p$, up to 0.938) ratio of the nanostructure is required, which means the gap between two nanorods needs to be ultra small (about 20 nm), as shown in the table in Fig. 1c. This requires high fabrication accuracy, but on the other hand, provides high resolution. The periodicity is close to the wavelength, so it is possible to form pixels that are much smaller than those of conventional chemical pigment-based methods.

**2.1.2 Polarization-dependent nanoantennas.** Polarization dependent color filtering and imaging provides another degree of freedom to manipulate color information,[35,36] which is important and has potential applications in many fields. First of all, it can be applied to polarization-related measurements, such as the birefringence measurements of cancerous tissues[65] and other bio-sensing applications. Secondly, it can improve data storage efficiency by having two different resonances for a single structure. The polarization dependence could at least double the information capacity by recording the data in different polarization states. In addition, it can also be useful in security applications by patterned surfaces that have concealed messages that can be read out only through the right combination of polarizers.

Due to the circular symmetry of the structures, the nanorod array responds equally to different polarized incident lights. However, the polarization dependence of the plasmonic nanostructures can also be utilized in color filtering and imaging applications. Polarization dependence of plasmonic nanostructures has been well studied in the past few years. For instance, nanostructures composed of metallic crosses with different arm lengths[35] exhibit strong dependence on the polarization states. As shown in Fig. 2a, b, only either vertical or horizontal polarized incident light can excite the LSPR of their corresponding arms, so that they have different transmission spectra and render different colors. At the arbitrary polarization angle $\varphi$, the transmission spectra is a linear superposition of the vertical and horizontal states, represented as

$$T(\varphi,\lambda) = T_V(\lambda)\sin^2\varphi + T_H(\lambda)\cos^2\varphi \quad (4)$$

where $T_V(\lambda)$ and $T_H(\lambda)$ are the transmittances for the light polarized vertically and horizontally. An optimized design of Al cross nanostructure[35] can be a yellow color filter for incident polarization along their short arms while being a blue filter for incident polarization along the long arms. With the controlled position and rotating angle of these elements, it can achieve active polarized images. Fig. 2c(ii–v) shows a sample of acronym "LSP". The cross nanoantennas composing the letters are identical to those in the background area, but rotated 90°. Therefore, for the vertical and horizontal polarized incidence, the letters show a different color from the background, but when the incident light is polarized 45°, the color difference is eliminated. Fig. 2c(vi–xi) shows another example, that of the cross nanoantennas that are patterned with a rotating angle $\theta(x) = 180°x/L$, where $x$ is the spatial coordinate and $L$ is the extent of the sample in the $x$ direction. As the incident polarization angle varies, the transmitted color image along the $x$ direction also moves like a wave. Moreover, the practical application of this plasmonic polarization dependent color filter has been successfully demonstrated by the bright field polarized imaging of a birefringent plastic film, and on chicken breast tissue with the birefringent effect of the muscle fibers.

Similar to the cross structures, pixels consisting aluminum (Al) elliptical nano-disks or a coupled nano-square pair with complementary holes at the bottom Al layer,[36] as shown in Fig. 2e, can also create different images with different polarized incident light (Fig. 2f). The nanostructure can provide abundant color in a full visible range. The application of these polarization dependent disks–holes nanostructures is further discussed in section 2.3.1.

**2.1.3 Structural color from one-dimensional (1D) metallic grating.** Efficiency is always an important parameter for practical applications. Metallic gratings,[32,48,53,66–76] which are also highly wavelength selective, are good candidates for highly efficient optical elements. A high transmission subtractive color filter with an ultrathin 1D silver (Ag) grating with subwavelength periodicity[67] is shown in Fig. 3a. Counter-intuitively,

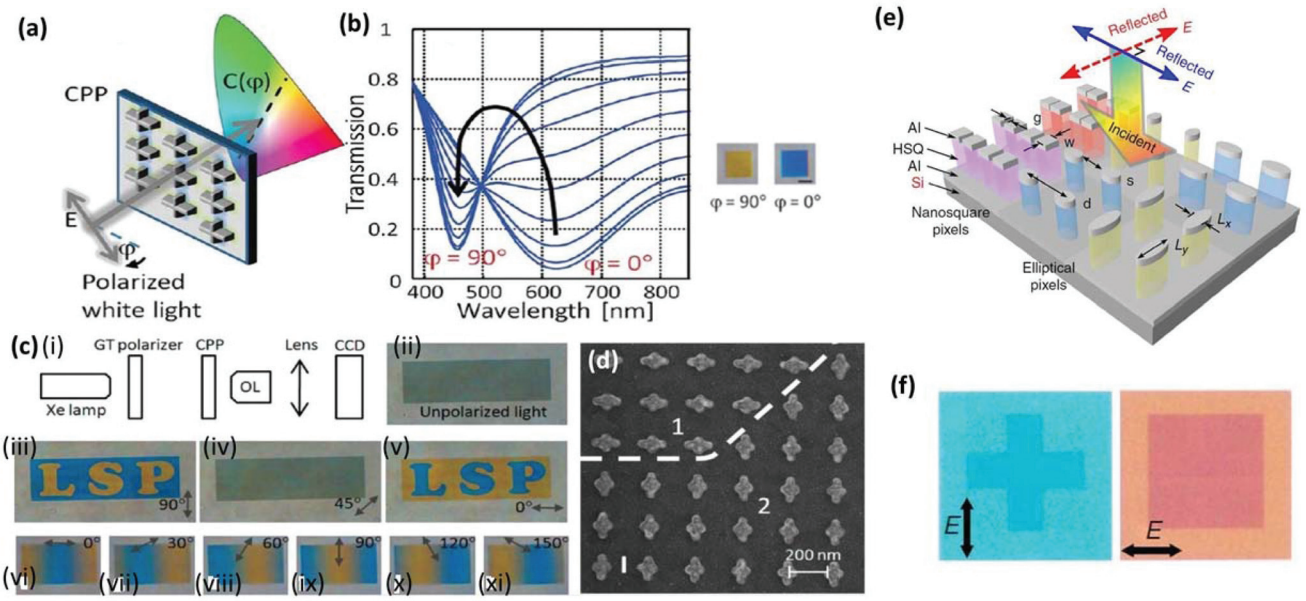


**Fig. 2** (a–c) Conversion of the polarization state to a visible color by cross nanoantennas: (a) polarized white light is color filtered by the LSPs on the arms of the cross nanoantennas; the output color results from the additive color mixing of the filtering functions of the two arms of the cross. (b) Simulated transmission spectra for linearly polarized illumination with the polarization angles ranging from $\varphi$ = 0°, at which yellow is blocked, to $\varphi$ = 90°, at which blue is blocked, in steps of 10°. (c(i)–(xi)) c(i) Schematic representation of the experimental setup. c(ii)–(v) Transmission images of the LSP pattern sample for (ii) unpolarized incident light, (iii) 90°, (iv) 45° and (v) 0° polarized light. c(vi)–(xi) Transmission images of the twisted sample for 0°–90° polarized light in steps of 30°. (d) SEM image of a part of the LSP sample. (d) Schematic diagram of polarization dependent nanostructures with elliptical nano-pillars and coupled nano-square pair pillars with Al on top and at the bottom. (e) Schematic diagram of polarization dependent nanostructures with Al elliptical nano-disks and coupled nano-square pair pillars with corresponding holes at the bottom Al layers. (f) Optical image of the same area formed from elliptical pixels with different linear polarized incident light. (a–d) Reproduced with permission.[35] Copyright 2012, ACS. (e, f) Reproduced with permission.[36] Copyright 2014, NPG.

an extraordinary low transmission (ELT) effect arises, resulting from the hybridization of LSPR and short-range surface plasmon polaritons. The ELT effect leads to a dip in the transmission spectrum. Simultaneously, since the Ag is optically thin the transmittance at off resonance wavelengths is high, which enables this nanostructure to be an efficient subtractive color filter. The efficiency of this simple 1D plasmonic grating filter would be 60–70%, which is very efficient among subtractive color filter designs.

On the other hand, high efficient additive color filters are greatly valuable as well. An Al grating[68] with a high-index dielectric waveguide layer can provide an efficiency of over 70% at transmission peak. The color filtering is achieved by means of the guided mode resonance (GMR) effect.[77,78] The GMR between the diffracted modes of grating and the guided modes of the planar dielectric waveguide (with Al grating as the upper cladding and a quartz substrate as the lower cladding) is readily induced as long as phase matching is achieved between them. The transmission is substantially increased when the incident wave constructively interferes with this coupled mode. Furthermore, as shown in Fig. 3c, a similar nanostructure but with a low-index buffer layer between the metal grating and high-index waveguide layer was reported with an improved transmittance of nearly 90%.[69] The thickness of the buffer layer can control the loss of the guided mode in metallic gratings, which can be explained by the theory of metal cladding dielectric waveguide.[79] Therefore, this nanostructure with a buffer layer can achieve narrow band resonances and high efficiency in the transmission spectra. This characteristic of high and sharp peaks is suitable for producing colors with high purity.

The resonance within the metal–insulator–metal (MIM) structures[32,45,70,71,80–84] can be used to filter white light into individual colors as well. The most important limitation of the MIM color filters is their low transmittance, so it is valuable to introduce diffractive effects into MIM structures to improve their efficiency. In Fig. 3e, a MIM grating is constructed by Al–ZnSe–Al resonators. The bottom Al grating is used to couple the incident light into the plasmon waveguide modes by diffraction, and the top Al grating reconverts the confined plasmon into propagating waves by scattering the light to far field in the forward direction, while the ZnSe layer ensures the efficient coupling of SP modes at the top and bottom Al layers. This photon–plasmon–photon conversion efficiently enhances the transmission at a specific wavelength. The periodicity of this MIM grating varies from 200 nm to 400 nm to achieve arbitrary colors; such a small periodicity also helps attaining high resolution for color image and display (in Fig. 3f).

Overall, the most significant advantage of plasmonic grating color filters and images among the plasmonic nanostructures is their high efficiency (usually 60% to 90%). For

 

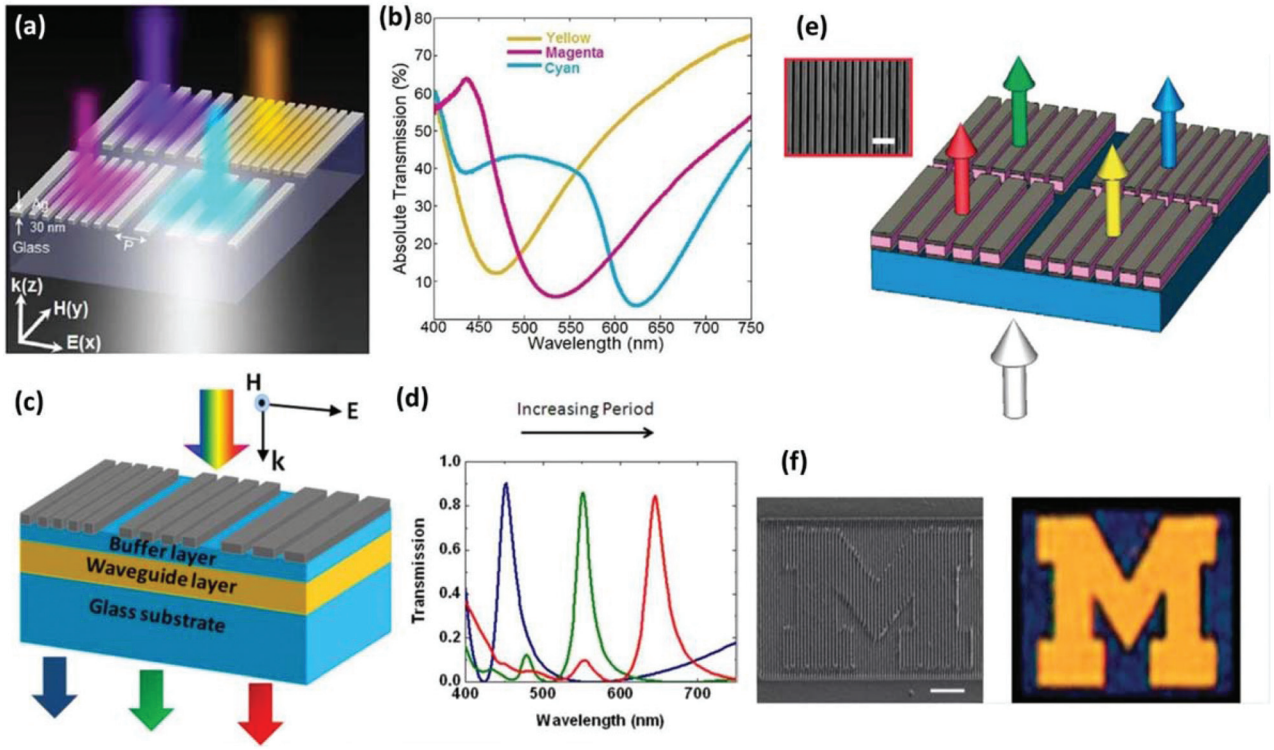


**Fig. 3** (a) Schematic diagram of the grating color filter of 30 nm thick Ag grating with different periods. (b) Measured TM transmission spectra of yellow, magenta and cyan for the structure in (a). (c) Schematic of the grating color filter structure with a buffer layer. (d) Simulated transmission spectra of RGB for the structure in (c). (e) Schematic diagram of the MIM grating color filter. (f) SEM image and optical microscopy image of the pattern "M" formed by the structure in (e) illuminated by white light. (a, b) Reproduced with permission.[67] Copyright 2013, NPG. (c, d) Reproduced with permission.[69] Copyright 2011, AIP Publishing LLC. (e, f) Reproduced with permission.[71] Copyright 2010, NPG.

those grating nanostructures coupled with guided modes, the bandwidth of resonance can be very narrow (with FWHM of 30 nm[69]), so that the filtered color can be pure. The spatial resolution of these nanostructures is also ultrahigh, close to the diffraction limit.[67,71] The period of grating can be minimised to half wavelength, and the length of grating can also be subwavelength, evolving to nanosquare arrays or so-called 2D gratings. Another characteristic of 1D grating is the polarization dependence. Only transverse magnetic (TM) waves (the electric field is perpendicular to the grating direction) can be filtered, while the transverse electric (TE) waves (the electric field is parallel to the grating direction) are mostly reflected or transmitted. Therefore they can actively work for many polarization-related applications as discussed in section 2.1.2.

### 2.2 Structural color from propagating surface plasmon

As discussed in section 2.1, the LSPR in metallic nanoantennas produces peaks in the reflection spectrum and dips in the transmission spectrum. According to the Babinet's principle,[85] the complements of these nanoantennas, which are the hole arrays in metal films, would result in dips in the reflection spectra and peaks in the transmission spectra. While nanoantenna arrays can work as subtractive color filters in the transmission mode, the nanohole arrays on metallic films can work as additive filters, which are needed in many imaging and display applications.

Considering a single hole in a metallic film, the transmission efficiency should be proportional to $(r/\lambda)^4$, where $\lambda$ is the incident wavelength and $r$ is the radius of the hole.[86,87] It means that the transmission of a subwavelength hole would be extremely low. However, the periodic metallic structures can provide the momentum for converting the incident light into SPs, so that the hole arrays on the metal film can give rise to the EOT effect.[19,20,22] In the past few years, the hole arrays had been theoretically and experimentally[88–107] studied in many aspects, such as the selective extraordinary transmission for color filtering. The wavelength of transmission peak $\lambda_{max}$ depends on the periodicity and the constituents of the hole arrays. At normal incidence, for the square array

$$\lambda_{max} = \frac{a}{\sqrt{i^2 + j^2}} \sqrt{\frac{\varepsilon_m \varepsilon_d}{\varepsilon_m + \varepsilon_d}} \quad (5)$$

and for the hexagonal array

$$\lambda_{max} = \frac{a}{\sqrt{\frac{4}{3}(i^2 + ij + j^2)}} \sqrt{\frac{\varepsilon_m \varepsilon_d}{\varepsilon_m + \varepsilon_d}} \quad (6)$$

where $a$ is the periodicity of the array, $\varepsilon_m$ and $\varepsilon_d$ are the relative permittivities of the metal and dielectric material, and $i$

and $j$ are the scattering orders of the array.[86,108,109] Considering the interference of the scattering losses of the holes and the Fano-type interaction,[62,110] $\lambda_{max}$ would be slightly blue shifted. Based on the interaction of these modes, the hole arrays can be designed for transmitted color filters.

In particular, for the lowest order mode ($i = \pm 1$, $j = 0$), the SPR peak wavelength of the hexagonal array is smaller than that of the square array with the same period and material. Moreover, the wavelength interval of the transmission peak between the first two modes of a hexagonal array is also larger, which makes the hexagonal array more favorable for reducing the color cross-talk and improving the purity of the color. To a lesser extent, the shape of holes also affects the color, as shown in Fig. 4a, b. The triangular hole arrays give narrower resonance peaks than the circular hole arrays, but with lower efficiency. After comparing them, it is also found that lattice construction has a larger influence on the hole shapes. Interestingly, the hexagonal array performs much better in building a full color map.

In experiments, the metallic film with a hole array is usually fabricated on a glass substrate, which leads to an asymmetric dielectric environment. Therefore, the two SP modes on both sides are resonant at different wavelengths, which would reduce the color purity due to the peaks overlapping. Owing to such asymmetry, a momentum mismatch also results in an inefficient coupling between the two sides and then a moderate transmittance. In order to deal with this, an index-matching layer is used to coat the air side.[108] As an example shown

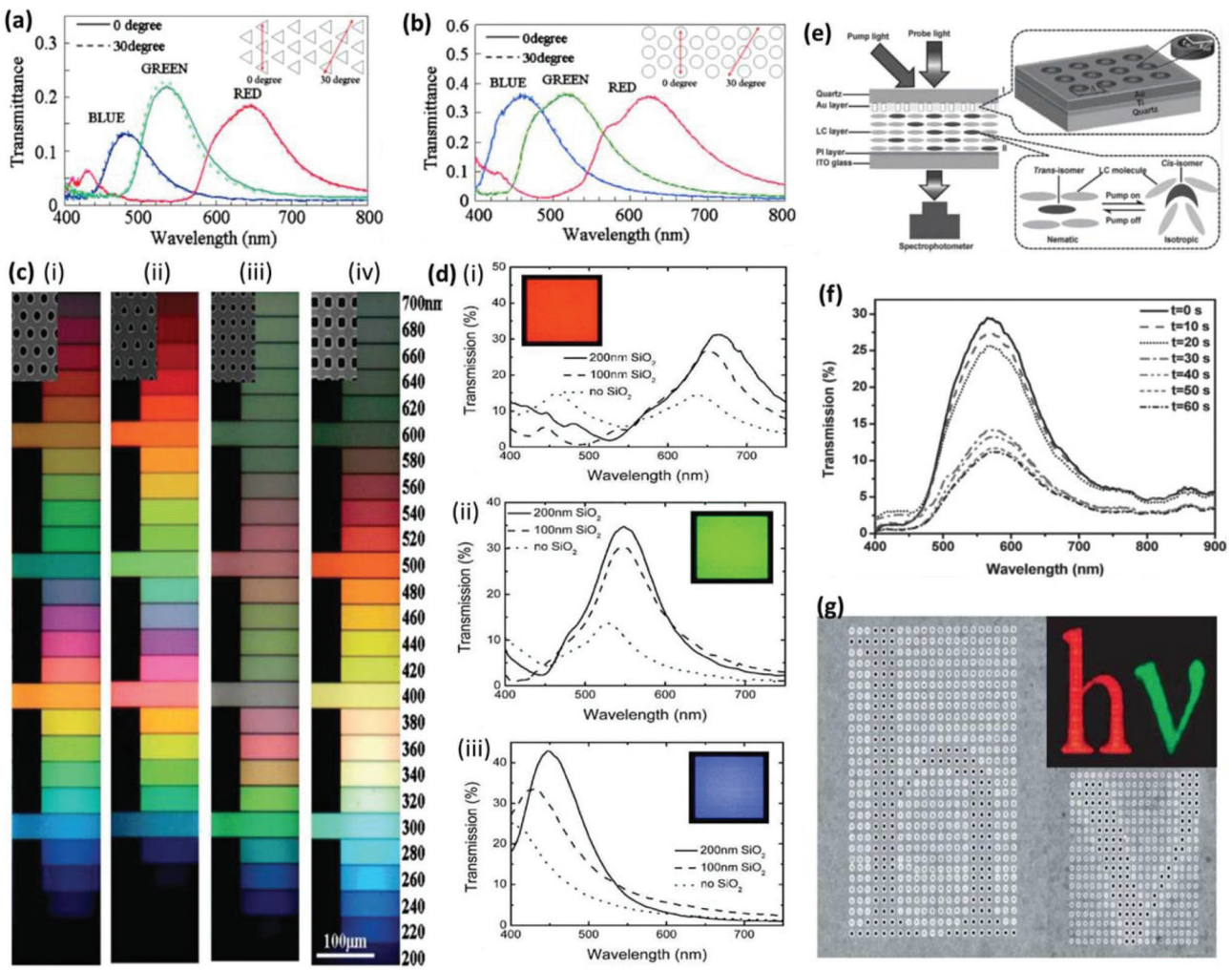


**Fig. 4** (a–b) Polarization dependence of the transmission spectra of RGB color filters with (a) triangular holes and (b) circular holes in hexagonal array. (c(i)–(iv)) Optical microscope images of Al color filters with (i) circular holes in the hexagonal array, (ii) triangular holes, (iii) circular holes in the square array, and (iv) square holes. (d(i)–(iii)) Measured transmission spectra of RGB color filters of circular hole arrays, with no cap layer, 100 nm and 200 nm $SiO_2$ cap layers. (e) Schematic of the sample structure and experimental setup for color filters with LC layers. The zoom-in part I shows the fabricated square pattern of Au AAAs, and the zoom-in part II shows the working mechanism of the optical driving process in LCs. (f) The evolution of the transmission spectra as a function of time using the UV pump for the color filter with an aperture size of 120 nm. (g) Holes in a dimple array generating the letters "*hv*" in transmission, with the periods of 550 nm (red color) and 450 nm (green color). (a–c) Reproduced with permission.[111] Copyright 2011, AIP Publishing LLC. (d) Reproduced with permission.[108] Copyright 2010, OSA. (e, f) Reproduced with permission.[47] Copyright 2012, John Wiley and Sons. (g) Reproduced with permission.[86] Copyright 2007, NPG.

 

in Fig. 4d, the transmittance was efficiently improved in the presence of an $SiO_2$ layer in comparison with the case of the absence of $SiO_2$.

As indicated by eqn (1) and (2), the transmission peak could be readily modulated by varying the refractive index of the environment. Recently, an active plasmonic color filter was introduced by overlaying photoresponsive liquid crystals (LCs) onto gold (Au) annular aperture arrays (AAAs),[47] as shown in Fig. 4e. The photochromic LC molecules would change their form upon UV irradiation, and further generate a photo-induced refractive index modulation. The transmittance could be greatly reduced as shown in Fig. 4f. Through further improving the tunability of plasmonic color filters with active optical control, an active display might be possible if the RGB compositions could be separately controlled.

The resolution of the metallic hole arrays is much higher than that of chemical pigments, but cannot reach the diffraction limit yet. For example, a color filter with different structures[111] is shown in Fig. 4c, while an image of "*hν*" is displayed with square hole arrays[86] in Fig. 4g. The periodicities are all larger than half of the corresponding wavelength, and are sometimes almost comparable to the wavelength.

Overall, the resolution of these nanohole arrays can already satisfy the requirements of most practical applications, with just a last step to the theory limitation. And they can also provide a variety of colors with promising visual effects, as shown in Fig. 4c. However, the transmission efficiency of nanohole arrays is relatively low compared to those color filters utilizing grating nanostructures.

### 2.3 Structural color from the plasmonic mode coupling

**2.3.1 Structural color from nanodisks-nanoholes.** In previous sections we have introduced some representative studies on color filtering and imaging, based on either localized or propagating SPs. However, in terms of resolution color imaging, there is still plenty of room for improvement in approaching the diffraction limit since the plasmonic nanostructures discussed previously (nanoantenna arrays, hole arrays, 1D gratings) have pixel sizes comparable to the wavelength. Here, a coupled plasmonic nanostructure which can produce pixels smaller than half-wavelength is introduced. The representative nanostructure contains a metallic nanodisk suspended on top of a dielectric pillar and a complementary metallic hole as a back reflector.[33,36,112–115] The top disks provide LSPRs and the back reflector provides propagating SPs, and the height of the dielectric pillars determines the coupling between them. It has been used for ultrahigh and uniform surface-enhanced Raman scattering,[114] and has demonstrated an extraordinary light transmission effect with a transparent substrate.[113] A high resolution nano-printing technology at the diffraction limit was reported based on this nanostructure,[33] by depositing a thin layer of Au–Ag on hydrogen silsesquioxane (HSQ) pillars on a silicon substrate. By manipulating the separation between the pillars and the sizes of the metal top disks, the coupling between the resonances of disks and the back reflector can be tuned to affect the reflected color.

As shown in Fig. 5a, b, a color map is achieved by nanostructures with different gap sizes ($g$) and disk sizes ($D$), pro-

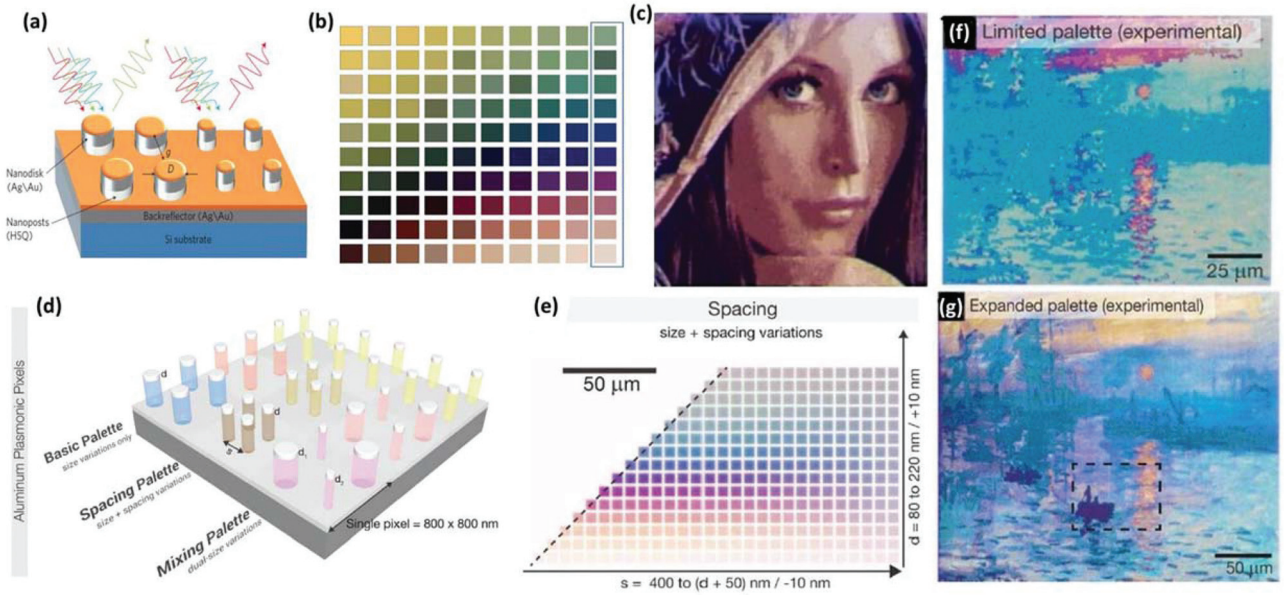


**Fig. 5** (a) Plasmonic color pixels composed of isolated Au/Ag nanodisks structures set against a back reflector. (b) Full color palettes with the disk size $D$ = 50–140 nm, gap size $g$ = 30–120 nm produced by pixels in (a). (c) Optical micrographs of the Lena image produced by pixels in (a). (d) Plasmonic color pixels composed of Al nanodisks with back reflectors of varying disk size palettes, varying disk sizes and spacing palettes and mix-disks palettes. (e) Full color palettes for pixels in (d). (f–g) Reproduction of Monet's *Impression, Sunrise* using (f) basic colors and (g) the expanded colors in (e). (a)–(c) Reproduced with permission.[33] Copyright 2012, NPG. (d–g) Reproduced with permission.[112] Copyright 2014, ACS.

viding also some really dark colors. It should be noted that the periodicity ($D + g$) varies from only 80 to 260 nm. In Fig. 5c, an image of *Lena* is produced by nanostructures with the same periodicity (125 nm) and different disk sizes. Such a small size of nanostructure ensures a resolution at the optical diffraction limit. To enrich the color gamut and increase the practicality of this nano-printing technology, the constituent materials Au and Ag are replaced by Al, which is a preferable metal for plasmonic color printing because of its neutral tint, durability, high reflectance in the visible regime, and low cost. With varied gaps and disk sizes, individual pixels are constructed by mixing disks of different sizes.[112] To complement the limited color palette produced by just modifying the gap and disk sizes, dual-size-disk pixels (2 × 2 disks array mixed with different sizes) are constructed, which greatly increased the range of colors and provided an approach for plasmonic color mixing (Fig. 5d, e). The comparison of a "basic" color palette by varying just the Au–Ag disk sizes and the "color-mixing" palette is shown in the micrographs in Fig. 5f, g. Color mixing provides an accurate reproduction of Monet's *Impression, Sunrise* painting that was poorly reproduced by the primary plasmonic color palette. Further research based on the disk-and-back-reflector-coupled nanostructures realizes 3D plasmonic stereoscopic prints utilizing their polarization dependence.[36] Using biaxial color pixels composed of elliptical nanodisk–hole structures (shown in Fig. 2e) can independently control the reflected spectra of orthogonal polarized incident light, so that two different color images can be encoded into the same area. Therefore, the stereoscopic effects can be achieved by fine modulation of the differences between the two images with different polarization.

**2.3.2 Structural color from other plasmonic nanostructures.** Plasmonic nanostructures for color filtering and imaging can also be achieved based on other characteristics and mechanisms.[34,115,116] For example, a MIM nanostructure containing Au nanodisk arrays hovering on a Au film with a thin dielectric layer in between, is capable of supporting gap-surface plasmons (GSPs).[115,117,118] By tuning the size of disks and the thickness of the dielectric layer, the reflected color can be tuned flexibly (Fig. 6a, b). This nanostructure with GSPs has its own advantages compared to many other plasmonic color nanostructures. Firstly, the reflection spectra are insensitive to the incident angle, which is valuable in practical applications. Secondly, while the colors of most plasmonic nanostructures are sensitive to the environmental index, this nanostructure can endure a cover of transparent dielectric overlay without shifting much in color. In Fig. 6c, an optical microscopy image is shown to compare the colors of uncovered (left) and dielectric covered (right) parts of the color printing, and the overall color image remains except for a slight contrast variation. Therefore, this plasmonic color device can be protected by coating a transparent layer without destroying the color, which enables its ambient usability.

Another incident angle independent case is based on Fabry–Perot (FP) cavity modes.[34] The structure is shown in Fig. 6d, and the dimensions and periodicity of the structure have been designed to avoid the plasmonic modes excitation relying on grating coupling, which is highly dependent on the incident angles. Instead, the nanostructures concentrate light into the silica nano-grooves based on light funnelling of FP cavity modes. At the designed wavelength, the absorbance can

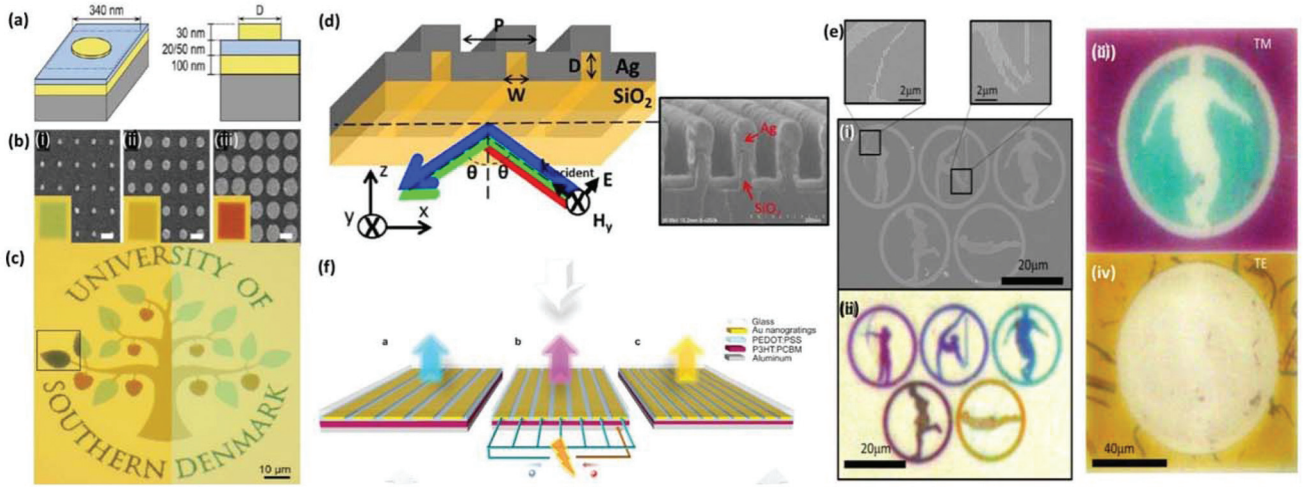


**Fig. 6** (a) Schematic views of a unit cell of a MIM structure with Au (yellow) nanodisks on the $SiO_2$ (blue) layer and the Au layer. (b(i)–(ii)) SEM images of nanodisks with average sizes of (i) 80, (ii)120, and (iii) 270 nm. (c) Optical microscopy images with pixels in (a) comparing an uncovered color print (left) and the same print (right) after covering the sample with 100 nm of PMMA. (d) Schematic of the light funnelling nanostructure and the corresponding SEM image. (e(i)–(iv)) The (i) SEM images and (ii) optical images under white light illumination of fabricated Olympic rings. (iii) TM and (iv) TE polarized light illuminating image of one of the Olympic rings. (f) Schematic of dual-function devices for both color filtering and electrical power generation. (a–c) Reproduced with permission.[115] Copyright 2014, ACS. (d), (e) Reproduced with permission.[34] Copyright 2013, NPG. (f) Reproduced with permission.[32] Copyright 2011, ACS.

 

reach over 90% within a ±90 degree angle range for specific structure dimensions, so that it performs well as an angle-independent subtractive reflective color filter. The periodicity of this plasmonic nanostructure is also beyond the diffraction limit of light, and thus it can produce polarization-dependent high resolution images, as shown in Fig. 6e.

In addition, the plasmonic color filter can also be integrated with organic solar cells.[32] As shown in Fig. 6f, the MIM nanostructure contains Au nano-grating on the top and an Al film at the bottom, which serve not only as a plasmonic color filter, but also as electrodes for the organic photovoltaic (OPV) cells. By manipulating the periodicity of grating and the thickness of the photoactive layer, the incident light at a specific wavelength can be directly absorbed and then transferred into photocurrents by the OPV structure instead of being wasted as heat, which indicates the great potential of plasmonic nanostructures in electrooptic applications.

## 3. Summary and outlook

We have reviewed the recent development of plasmonic colors generated by nanostructures. Compared to the conventional pigments and the non-plasmonic structural colors, plasmonic color offers more advantages including ultrasmall dimensions, impressive optical response, wide color tunability and compatibility for device integration. The nano-scaled size of plasmonic structures enables image printing at high resolutions, even beyond the optical diffraction limit. Most structures simply contain one or several ultrathin layers of metallic/dielectric materials, so that their thickness is only tens or hundreds of nanometers. This thin geometry makes it easy to integrate them with miniaturized devices. The well-controlled plasmonic resonance also provides a wide color range and accurately distinguished colors. Moreover, the diversity of plasmonic nanostructures contributes in achieving specific targets, such as high efficiency in transmission or reflection, narrower band-width for purer colors, reduced incident angle dependence, tunable polarization applications, and electro-optic modulations.

Although plasmonic nanostructures have so many advantages and great potential in next generation color relevant applications, the first commercial applications would require a drastic reduction in patterning costs. Fabrication methods such as EBL and FIB are necessary to create master templates from which high-throughput replication processes such as nanoimprint can be used to create a large volume of copies. The commonly used plasmonic materials, Au and Ag, are also expensive for mass production, leading to the recent trend towards using Al, which is also CMOS compatible. In addition to cost reduction, the performance of plasmonic devices needs to be comparable to, or better than, existing technologies. For instance, in the application of plasmonic color filters for digital imaging products, the limiting factor is still the insufficient transmittance when compared to pigment-based filters. Hence, while many novel phenomena have been reported in the literature, a strong need now is to significantly improve the optical performance of plasmonic color structures.

In summary, plasmonic nanostructures show great potential in the development of color filtering, high-resolution display and imaging, optical data storage and security. With improved low-cost fabrication technology, they are slated to offer improved performance and lower cost in applications ranging from digital displays, imaging sensors, molecular sensing to optical security devices and optical data archival.

## Acknowledgements

The authors acknowledge the support from the National University of Singapore (grant R-263-000-A45-112).

## References

1 Y. Huo, C. C. Fesenmaier and P. B. Catrysse, *Opt. Express*, 2010, **18**, 5861.
2 H. Koo, M. Chen and P. Pan, *Thin Solid Films*, 2006, **515**, 896.
3 M. C. Gather, A. Köhnen, A. Falcou, H. Becker and K. Meerholz, *Adv. Funct. Mater.*, 2007, **17**, 191.
4 E. Abbe, *Proc. Bristol Nat. Soc.*, 1874, **1**, 200.
5 P. Vukusic and J. R. Sambles, *Nature*, 2003, **424**, 852.
6 M. Sinivasarao, *Chem. Rev.*, 1999, **99**, 1935.
7 J. Huang, X. Wang and Z. L. Wang, *Nano Lett.*, 2006, **6**, 2325.
8 T. S. Kustandi, H. Y. Low, J. H. Teng, I. Rodriguez and R. Yin, *Small*, 2009, **5**, 574.
9 P. Vukusic, J. R. Sambles, C. R. Lawrence and R. J. Wootton, *Proc. R. Soc. London, Ser. B*, 1999, **266**, 1402.
10 S. Kinoshita, S. Yoshioka and K. Kawagoe, *Proc. R. Soc. London, Ser. B*, 2002, **269**, 1417.
11 H. Ghiradella, *Appl. Opt.*, 1991, **30**, 3492.
12 C. R. Lawrence, P. Vukusic and J. R. Sambles, *Appl. Opt.*, 2002, **41**, 437.
13 L. Cao, P. Fan, E. S. Barnard, A. M. Brown and M. L. Brongersma, *Nano Lett.*, 2010, **10**, 2649.
14 M. Khorasaninejad, N. Abedzadeh, J. Walia, S. Patchett and S. S. Saini, *Nano Lett.*, 2012, **12**, 4228.
15 K. Seo, M. Wober, P. Steinvurzel, E. Schonbrun, Y. Dan, T. Ellenbogen and K. B. Crozier, *Nano Lett.*, 2011, **11**, 1851.
16 H. Park, Y. Dan, K. Seo, Y. J. Yu, P. K. Duane, M. Wober and K. B. Crozier, *Nano Lett.*, 2014, **14**, 1804.
17 V. R. Shrestha, S.-S. Lee, E.-S. Kim and D.-Y. Choi, *Sci. Rep.*, 2014, **4**, 4921.
18 Z. Wu, D. Lee, M. F. Rubner and R. E. Cohen, *Small*, 2007, **3**, 1445.
19 T. Ebbesen, H. Lezec, H. Ghaemi, T. Thio and P. Wolff, *Nature*, 1998, **86**, 1114.
20 S. Enoch, E. Popov, M. Neviere and R. Reinisch, *J. Opt. A: Pure Appl. Opt.*, 2002, **4**, 83.

21 W. T. Chen, K.-Y. Yang, C.-M. Wang, Y.-W. Huang, G. Sun, I.-D. Chiang, C. Y. Liao, W.-L. Hsu, H. T. Lin, S. Sun, L. Zhou, A. Q. Liu and D. P. Tsai, *Nano Lett.*, 2014, **14**, 225.
22 W. Fan, S. Zhang, B. Minhas, K. J. Malloy and S. R. J. Brueck, *Phys. Rev. Lett.*, 2005, **94**, 033902.
23 G. Li, M. Kang, S. Chen, S. Zhang, E. Y.-B. Pun, K. W. Cheah and J. Li, *Nano Lett.*, 2013, **13**, 4148.
24 L. Meng, D. Zhao, Q. Li and M. Qiu, *Opt. Express*, 2013, **21**, A111.
25 N. Yu, F. Aieta, P. Genevet, M. A. Kats, Z. Gaburro and F. Capasso, *Nano Lett.*, 2012, **12**, 6328.
26 N. Yu, P. Genevet, M. A. Kats, F. Aieta, J.-P. Tetienne, F. Capasso and Z. Gaburro, *Science*, 2011, **334**, 333.
27 X. Chen, L. Huang, H. Mühlenbernd, G. Li, B. Bai, Q. Tan, G. Jin, C.-W. Qiu, S. Zhang and T. Zentgraf, *Nat. Commun.*, 2012, **3**, 1198.
28 S. J. Tan, X. M. Goh, Y. M. Wang, J. K. W. Yang and J. Teng, *J. Mol. Eng. Mater.*, 2014, **02**, 1440011.
29 T. Xu, H. Shi, Y.-K. Wu, A. F. Kaplan, J. G. Ok and L. J. Guo, *Small*, 2011, **7**, 3128.
30 Y. Yu, L. Wen, S. Song and Q. Chen, *J. Nanomater.*, 2014, **2014**, 212637.
31 H. Liu and P. Lalanne, *Nature*, 2008, **452**, 728.
32 H. J. Park, T. Xu, J. Y. Lee, A. Ledbetter and L. J. Guo, *ACS Nano*, 2011, **5**, 7055.
33 K. Kumar, H. Duan, R. S. Hegde, S. C. W. Koh, J. N. Wei and J. K. W. Yang, *Nat. Nanotechnol.*, 2012, **7**, 557.
34 Y.-K. R. Wu, A. E. Hollowell, C. Zhang and L. J. Guo, *Sci. Rep.*, 2013, **3**, 1194.
35 T. Ellenbogen, K. Seo and K. B. Crozier, *Nano Lett.*, 2012, **12**, 1026.
36 X. M. Goh, Y. Zheng, S. J. Tan, L. Zhang, K. Kumar, C. W. Qiu and J. K. W. Yang, *Nat. Commun.*, 2014, **5**, 5361.
37 A. V. Zayatsa, I. I. Smolyaninovb and A. A. Maradudinc, *Phys. Rep.*, 2005, **408**, 131–314.
38 E. Ozbay, *Science*, 2006, **311**, 189.
39 E. Laux, C. Genet, T. Skauli and T. W. Ebbesen, *Nat. Photonics*, 2008, **2**, 161.
40 W. L. Barnes, A. Dereux and T. W. Ebbesen, *Nature*, 2003, **424**, 824.
41 W. L. Barnes, *J. Opt. A: Pure Appl. Opt.*, 2006, **8**, 87.
42 H. Duan, H. Hu, K. Kumar, Z. Shen and J. K. W. Yang, *ACS Nano*, 2011, **5**, 7593.
43 H. Duan, H. Hu, H. K. Hui, Z. Shen and J. K. W. Yang, *Nanotechnology*, 2013, **24**, 185301.
44 Y. J. Liu, G. Y. Si, E. S. P. Leong, B. Wang, A. J. Danner, X. C. Yuan and J. H. Teng, *Appl. Phys. A*, 2012, **107**, 49.
45 K. Diest, J. Dionne, M. Spain and H. Atwater, *Nano Lett.*, 2009, **9**, 2579.
46 C. Saeidi and D. van der Weide, *Opt. Express*, 2014, **22**, 12499.
47 Y. J. Liu, G. Y. Si, E. S. P. Leong, N. Xiang, A. J. Danner and J. H. Teng, *Adv. Mater.*, 2012, **24**, 131.
48 M. J. Uddin and R. Magnusson, *IEEE Photonics Technol. Lett.*, 2012, **24**, 1552.
49 P. Zijlstra, J. W. M. Chon and M. Gu, *Nature*, 2009, **459**, 410.
50 G. Si, Y. Zhao, J. Lv, M. Lu, F. Wang, H. Liu, N. Xiang, T. J. Huang, A. J. Danner, J. Teng and Y. J. Liu, *Nanoscale*, 2013, **5**, 6243.
51 J. Do, M. Fedoruk, F. Jäckel and J. Feldmann, *Nano Lett.*, 2013, **13**, 4164.
52 L. L. Huang, X. Chen, H. Muhlenbernd, H. Zhang, S. Chen, B. Bai, Q. Tan, G. Jin, K.-W. Cheah, C.-W. Qiu, J. Li, T. Zentgraf and S. Zhang, *Nat. Commun.*, 2013, **4**, 2808.
53 J. J. Cowan, *Opt. Commun.*, 1972, **5**, 2.
54 S. Zou and G. C. Schatz, *Nanotechnology*, 2006, **17**, 2813.
55 V. A. Markel and A. K. Sarychev, *Phys. Rev. B: Condens. Matter.*, 2007, **75**, 085426.
56 C. Bohren and D. Huffman, *Absorption and Scattering of Light by Small Particles*, John Wiley & Sons, New York, 1983.
57 B. Auguie and W. L. Barnes, *Phys. Rev. Lett.*, 2008, **101**, 143902.
58 F. J. García de Abajo, *Rev. Mod. Phys.*, 2007, **79**, 1267.
59 R. W. Wood, *Philos. Mag.*, 1902, **4**, 396.
60 V. G. Kravets, F. Schedin and A. N. Grigorenko, *Phys. Rev. Lett.*, 2008, **101**, 087403.
61 K. Lee and P. Wei, *Small*, 2010, **6**, 1900.
62 M. Sarrazin, J.-P. Vigneron and J.-M. Vigoureux, *Phys. Rev. B: Condens. Matter*, 2003, **67**, 085415.
63 L. Shao, K. C. Woo, H. Chen, Z. Jin, J. Wang and H.-Q. Lin, *ACS Nano*, 2010, **4**, 3053.
64 C. J. Tang, P. Zhan, Z. S. Cao, J. Pan, Z. Chen and Z. L. Wang, *Phys. Rev. B: Condens. Matter*, 2011, **83**, 041402.
65 J. Strasswimmer, M. C. Pierce, B. H. Park, V. Neel and J. F. de Boer, *J. Biomed. Opt.*, 2004, **9**, 292.
66 Q. Chen, C. Martin and D. R. S. Cumming, *Plasmonics*, 2012, **7**, 755.
67 B. Zeng, Y. Gao and F. J. Bartoli, *Sci. Rep.*, 2013, **3**, 2840.
68 Y.-T. Yoon, C.-H. Park and S.-S. Lee, *Appl. Phys. Express*, 2012, **5**, 022501.
69 A. F. Kaplan, T. Xu and L. J. Guo, *Appl. Phys. Lett.*, 2011, **99**, 143111.
70 Y. Chen and W. Liu, *Opt. Lett.*, 2012, **37**, 1.
71 T. Xu, Y.-K. Wu, X. Luo and L. J. Guo, *Nat. Commun.*, 2010, **1**, 59.
72 D. C. Skigin and R. A. Depine, *Phys. Rev. Lett.*, 2005, **95**, 217402.
73 Z. Sun, Y. S. Jung and H. K. Kim, *Appl. Phys. Lett.*, 2003, **83**, 3021.
74 J. A. Porto, F. J. García-Vidal and J. B. Pendry, *Phys. Rev. Lett.*, 1999, **83**, 2845.
75 A. Barbara, P. Quémerais, E. Bustarret and T. Lopez-Rios, *Phys. Rev. B: Condens. Matter*, 2002, **66**, 161403.
76 N. Nguyen-Huu, Y.-L. Lo and Y.-B. Chen, *Opt. Commun.*, 2011, **284**, 2473.
77 N. Ganesh, A. Xiang, N. B. Beltran, D. W. Dobbs and B. T. Cunningham, *Appl. Phys. Lett.*, 2007, **90**, 081103.
78 D. W. Dobbs, I. Gershkovich and B. T. Cunningham, *Appl. Phys. Lett.*, 2006, **89**, 123113.

79 H. Nishihara, M. Haruna and T. Suhara, *Optical Integrated Circuits*, McGraw-Hill, New York, 1989.
80 P. Chen, R. Liang, Q. Huang, Z. Yu and X. Xu, *Opt. Express*, 2011, **19**, 7633.
81 L. Zhang, J. Hao, H. Ye, S. P. Yeo, M. Qiu, S. Zouhdid and C.-W. Qiu, *Nanoscale*, 2013, **5**, 3373.
82 Y.-T. Yoon and S.-S. Lee, *Opt. Express*, 2010, **18**, 5344.
83 L. Frey, P. Parrein, J. Raby, C. Pellé, D. Hérault, M. Marty and J. Michailos, *Opt. Express*, 2011, **19**, 13073.
84 A. F. Kaplan, T. Xu, Y. Wu and L. J. Guo, *J. Vac. Sci. Technol., B*, 2010, **28**, C6O60.
85 M. Born and E. Wolf, *Principles of Optics*, Cambridge University Press, Cambridge, 1999.
86 C. Genet and T. W. Ebbesen, *Nature*, 2007, **445**, 39.
87 H. A. Bethe, *Phys. Rev.*, 1944, **66**, 163.
88 L. Lin and A. Roberts, *Appl. Phys. Lett.*, 2010, **97**, 061109.
89 K. Walls, Q. Chen, S. Collins, D. R. S. Cumming and T. D. Drysdale, *IEEE Photonics Technol. Lett.*, 2012, **24**, 602.
90 H.-S. Lee, Y.-T. Yoon, S.-S. Lee, S.-H. Kim and K.-D. Lee, *Opt. Express*, 2007, **15**, 15457.
91 G. Si, Y. Zhao, H. Liu, S. Teo, M. Zhang, T. J. Huang, A. J. Danner and J. Teng, *Appl. Phys. Lett.*, 2011, **99**, 033105.
92 A. Degiron, H. J. Lezec, W. L. Barnes and T. W. Ebbesen, *Appl. Phys. Lett.*, 2002, **81**, 4327.
93 Y. M. Strelniker and D. J. Bergman, *Phys. Rev. B: Condens. Matter*, 1999, **59**, R12763.
94 E. Popov, M. Neviere, S. Enoch and R. Reinisch, *Phys. Rev. B: Condens. Matter*, 2000, **62**, 16100.
95 F. I. Baida and D. Van Labeke, *Opt. Commun.*, 2002, **209**, 17.
96 P. Lalanne, J. C. Rodier and J. P. Hugonin, *J. Opt. Pure Appl. Opt.*, 2005, **7**, 422.
97 V. Lomakin and E. Michielssen, *Phys. Rev. B: Condens. Matter*, 2005, **71**, 235117.
98 F. J. Garcia de Abajo, J. J. Saenz, I. Campillo and J. S. Dolado, *Opt. Express*, 2006, **14**, 7.
99 S.-H. Chang, S. K. Gray and G. C. Schatz, *Opt. Express*, 2005, **13**, 3150.
100 W. L. Barnes, W. A. Murray, J. Dintinger, E. Devaux and T. W. Ebbesen, *Phys. Rev. Lett.*, 2004, **92**, 107401.
101 J. Prikulis, P. Hanarp, L. Olofsson, D. Sutherland and M. Kall, *Nano Lett.*, 2004, **4**, 1003.
102 K. J. Klein Koerkamp, S. Enoch, F. B. Segerink, N. F. van Hulst and L. Kuipers, *Phys. Rev. Lett.*, 2004, **92**, 183901.
103 A. Degiron and T. W. Ebbesen, *J. Opt. Pure Appl. Opt.*, 2005, **7**, 90.
104 Y.-H. Ye and J.-Y. Zhang, *Opt. Lett.*, 2005, **30**, 1521.
105 Q.-J. Wang, J.-Q. Li, C.-P. Huang, C. Zhang and Y.-Y. Zhu, *Appl. Phys. Lett.*, 2005, **87**, 091105.
106 D. Egorov, B. S. Dennis, G. Blumberg and M. I. Haftel, *Phys. Rev. B: Condens. Matter*, 2004, **70**, 033404.
107 E. Altewischer, M. P. van Exter and J. P. Woerdman, *J. Opt. Soc. Am. B*, 2003, **20**, 1927.
108 Q. Chen and D. R. S. Cumming, *Opt. Express*, 2010, **18**, 14056.
109 H. F. Ghaemi, T. Thio, D. E. Grupp, T. W. Ebbesen and H. J. Lezec, *Phys. Rev. B: Condens. Matter*, 1998, **58**, 6779.
110 C. Genet, M. P. van Exter and J. P. Woerdman, *Opt. Commun.*, 2003, **225**, 331.
111 D. Inoue, A. Miura, T. Nomura, H. Fujikawa, K. Sato, N. Ikeda, D. Tsuya, Y. Sugimoto and Y. Koide, *Appl. Phys. Lett.*, 2011, **98**, 093113.
112 S. J. Tan, L. Zhang, D. Zhu, X. M. Goh, Y. M. Wang, K. Kumar, C.-W. Qiu and J. K. W. Yang, *Nano Lett.*, 2014, **14**, 4023.
113 W.-D. Li, J. Hu and S. Y. Chou, *Opt. Express*, 2011, **19**, 21098.
114 W.-D. Li, F. Ding, J. Hu and S. Y. Chou, *Opt. Express*, 2011, **19**, 3925.
115 A. S. Roberts, A. Pors, O. Albrektsen and S. I. Bozhevolnyi, *Nano Lett.*, 2014, **14**, 783.
116 J. Zhang, J.-Y. Ou, N. Papasimakis, Y. Chen, K. F. MacDonald and N. I. Zheludev, *Opt. Express*, 2011, **19**, 23279.
117 N. Liu, M. Mesch, T. Weiss, M. Hentschel and H. Giessen, *Nano Lett.*, 2010, **10**, 2342.
118 Y. Chu and K. B. Crozier, *Opt. Lett.*, 2009, **34**, 3.